Journal of ELECTRONIC MATERIALS, Vol. 45, No. 3, 2016
DOI: 10.1007/s11664-015-4270-y

Magnetic-Field Dependence of Thermoelectric Properties of Sintered $Bi_{90}Sb_{10}$ Alloy

MASAYUKI MURATA,[1,4] ATSUSHI YAMAMOTO,[1]
YASUHIRO HASEGAWA,[2] and TAKASHI KOMINE[3]

1.—iECO, National Institute of Advanced Industrial Science and Technology (AIST), 1-1-1 Umezono, Tsukuba, Ibaraki 305-8568, Japan. 2.—Faculty of Engineering, Saitama University, 255 Shimo-Okubo, Sakura, Saitama 338-8570, Japan. 3.—Faculty of Engineering, Ibaraki University, 4-12-1 Nakanarusawa, Hitachi, Ibaraki 316-8511, Japan. 4.—e-mail: m.murata@aist.go.jp

The magnetic-field dependence of the thermoelectric properties and dimensionless figure of merit (ZT) of a sintered $Bi_{90}Sb_{10}$ alloy were experimentally and theoretically evaluated. The Bi-Sb alloy was synthesized in a quartz ampule using the melting method, and the resultant ingot was then ground via ball milling. A sintered $Bi_{90}Sb_{10}$ alloy with a particle size in the range of several to several tens of micrometers was prepared using the spark plasma sintering (SPS) method. The magnetic-field dependence of the electrical resistivity, Seebeck coefficient, and thermal conductivity were experimentally evaluated at temperatures of 77–300 K for magnetic fields of up to 2.9 T. The results showed that ZT increased by 37% at 300 K under a 2.5-T magnetic field. A theoretical calculation of the magneto-Seebeck coefficient based on the Boltzmann equation with a relaxation time approximation was also performed. Hence, the experimental result for the magneto-Seebeck coefficient of the $Bi_{90}Sb_{10}$ alloy at 300 K was qualitatively and quantitatively explained. Specifically, the carrier scattering mechanism was shown to be acoustic phonon potential scattering and the carrier mobility ratio between the L- and T-points was found to be 3.3, which corresponds to the characteristics of a single crystal. It was concluded that the effect of the magnetic field on the Seebeck coefficient was demonstrated accurately using the theoretical calculation model.

Key words: Bi-Sb alloy, thermoelectrics, magneto-Seebeck effect, Boltzmann equation

INTRODUCTION

Thermoelectric materials with high performance in the room-temperature range are in considerable demand for practical applications, e.g., in cooling devices and low-temperature waste-heat recovery systems. While Bi-Te-based materials are already available for practical use in applications employing the room-temperature range, the prices of such modules can be reduced by replacing the costly Te with alternative, low-cost materials. Bi-Sb-based alloys are known to have high thermoelectric performance in the low-temperature range (at approximately 120 K);[1,2] however, their performance in the vicinity of room temperature is inferior to that of Bi-Te-based alloys. Further, nanostructured Bi-Sb materials such as thin films and nanowires have been studied actively, because their small effective masses are attractive for quantization.[3] In this study, the effect of a magnetic field B on the thermoelectric properties of Bi-Sb-based alloys is studied in order to identify methods to enhance the thermoelectric performance of these materials in the room-temperature range.

Application of B affects the electrical conductivity σ, Seebeck coefficient S, and thermal conductivity κ of Bi-Sb alloys, so that the dimensionless figure of

(Received June 1, 2015; accepted November 25, 2015; published online December 29, 2015)

merit ZT ($=\sigma S^2 T/\kappa$) is enhanced. Wolfe et al. have reported that the maximum ZT of a $Bi_{88}Sb_{12}$-alloy single crystal increases from 0.55 under non-B conditions at 120 K to 1.28 following application of an external B of 1.7 T at 220 K.[4] Furthermore, they reported that ZT = 0.84 even at 300 K, which is comparable to the ZT value of ~0.87 of the n-type Bi-Te-based alloy.[5] This suggests that the B effect on Bi-Sb alloys can be used effectively to enhance the thermoelectric performance of these materials in the vicinity of room temperature. It has also been reported that the temperature T drop of a Peltier element is enhanced by approximately 80 K under an external B induced by a permanent magnet.[6] Such a significant dependence on B in the case of a Bi-Sb alloy is very attractive with regard to thermoelectrics, and an accurate theoretical understanding is important in order to enhance the thermoelectric performance of devices containing this alloy, especially in the room-temperature range.

The ZT enhancement under B is primarily caused by an increase in the magneto-Seebeck coefficient.[4] Theoretical investigations of the magneto-Seebeck coefficient have not been well performed, although experimental results have been reported by many researchers.[4,7–11] For example, Thomas and Goldsmid have qualitatively explained the experimental result for the magneto-Seebeck coefficient of the Te-doped Bi-Sb alloy, using a calculation in which only the electrons of the non-parabolic band at the L point are considered.[12] In addition, our group has theoretically studied the magneto-Seebeck coefficient of Bi and Bi-Sb alloys using a calculation model in which three bands of the electrons and holes at the L point and the holes at the T point are considered.[13–15] However, quantitative agreement between the calculated and experimental results is not sufficient when the carrier neutral condition is applied.

Therefore, this study attempts to explain the experimental result for the magneto-Seebeck coefficient of the Bi-Sb alloy in a quantitative manner, using a theoretical calculation with a carrier neutral condition. A sintered $Bi_{90}Sb_{10}$ alloy with no strong anisotropy in its thermoelectric properties is prepared as a measurement sample. The individual B dependencies of the thermoelectric properties are measured experimentally, and are also calculated theoretically using the Boltzmann equation with a relaxation time approximation. In our previous paper, we calculated the magneto-Seebeck coefficient at 100 K, where the band structure does not change significantly.[15] On the other hand, this study focuses on the thermometric performance in the vicinity of room temperature; therefore, the band structure alteration should be considered, because the Bi-Sb alloy band structure has strong T dependence.[16] Thus, the band structure of the $Bi_{90}Sb_{10}$ alloy at 300 K is estimated from a lattice constant evaluated via x-ray diffraction (XRD), and also from the relationship between the band structure and lattice constant at 4.2 K. Three bands of the non-parabolic electrons and holes at the L point and the parabolic holes at the T point are considered in the magneto-Seebeck coefficient calculation.

EXPERIMENTAL

The base material used in this study, namely, a polycrystalline Bi-Sb alloy, was synthesized using the melting method. Bi of 99.99% purity and Sb of 99.999% purity were placed inside a quartz ampoule with an atomic ratio of 92.0:8.00. The vacuum-sealed quartz ampoule was set in a muffle furnace, and the Bi-Sb alloy was then synthesized at a T of 400°C, which is sufficiently higher than the $Bi_{92}Sb_8$ alloy melting point.[17] This T was maintained for 24 h. Then, T was decreased from 400°C to 290°C for the liquid line of the $Bi_{92}Sb_8$ alloy, at a rate of 1°C/min, and then from 290°C to 250°C for the solidus line at a very slow rate of 1°C/h. Finally, T was decreased from 250°C to room temperature at a rate of 1°C/min. A synthesized Bi-Sb alloy ingot, which was ca. 75 mm in length and ca. 7 mm in diameter, was cut into 14 pellets of 5-mm width along the longitudinal direction. The pellet cross sections were analyzed using energy dispersive x-ray spectroscopy (EDX) in order to determine the Sb concentration distribution. Unfortunately, the variation of the Sb concentration distribution along the longitudinal direction was large, ranging from 1% to 14%; this was because of the difference in the atomic weights of Bi and Sb. Therefore, six pellets from the top side (30 mm in length) were selected for sample preparation, because the Sb concentration distribution was stable at approximately 10%. These pellets were ground using dry ball milling at 450 rpm and for 30 min, using a Retsch S100 with a 25-mm-diameter ball and a 250-mL pot composed of agate. Then, the prepared powder was sintered using the spark plasma sintering (SPS) method at 200°C and 50 MPa for 10 min.

Figure 1 shows (a) a schematic diagram and (b) a photograph of the experimental set-up used to measure the B dependence of the thermoelectric properties. The $Bi_{90}Sb_{10}$ alloy sample had a rectangular parallelepiped shape with dimensions of $2.98 \times 2.99 \times 9.03$ mm^3. Two 0.4-mm-thick Cu plates were attached to both edges of the sample, as shown in the figures, to yield a temperature difference ΔT along the longitudinal direction. Silver paste (Diemat Sk100), which has high κ, was used to attach the Cu plates, and the paste was fixed at a T of 150°C, which was maintained for 30 min. Note that, although the importance of the diffusion boundary layer on the Bi-Te alloy (in order to prevent silver diffusion) has been reported,[18] the heating temperature in this study was sufficiently low to avoid this problem. Cu wires of 25-μm diameter were attached to both Cu plates using silver epoxy (Epotek H20E), which has strong

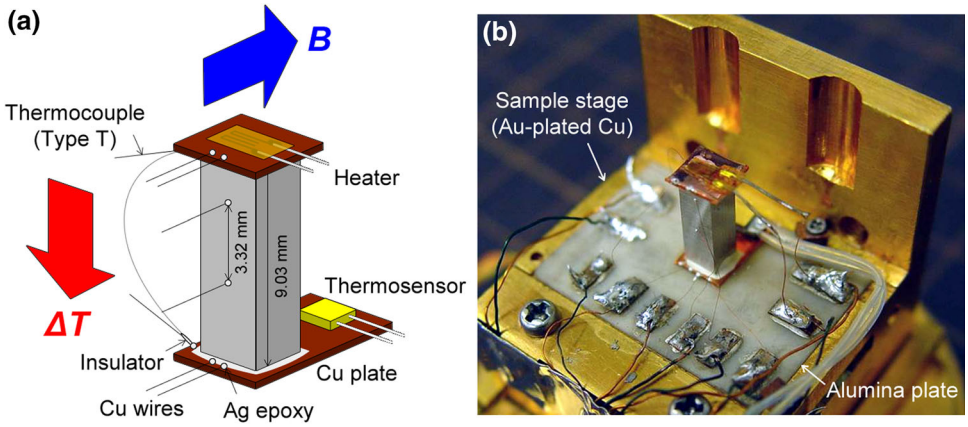

Fig. 1. (a) Schematic diagram and (b) photograph of experimental set-up used to measure magnetic-field dependence of thermoelectric properties.

adhesion force. For four-wire electrical resistance ρ measurement, two Cu wires were attached to the side of the sample with a gap of 3.32 mm, again using silver epoxy.

A 120-Ω heater was used to create the ΔT for the measurement of S, and was attached to the upper side of the Cu plate using a cyanoacrylate-based adhesive. A type-T differential thermocouple was also thermally attached to the two Cu plates using silver epoxy so that ΔT could be measured. The lower-side contact point of the differential thermocouple was insulated using a mixture of alumina powder and adhesive. The prepared sample was set on an alumina plate that was fixed on a sample stage composed of Au-plated Cu, and a Cernox temperature sensor was attached to the lower side of the Cu plate to measure the absolute T. All measurements of the thermoelectric properties were performed at T values of 77 K to 300 K, which were precisely controlled with a fluctuation of less than 1 mK using a Gifford–McMahon (GM) cooler and heater.[19] Further, these measurements were conducted in a vacuum atmosphere of the order of 10^{-4} Pa or less. The value of ρ was measured using the four-wire method with an alternative current (AC) supplied by a current source (Keithley 6221), and measured using a lock-in amplifier (SR 830) at a frequency of 11.234 Hz and an electrical current of 10 mA. The values of S and the thermal diffusivity α were simultaneously measured using the AC method[20] at an input frequency of 0.05 Hz. A B was applied transverse to the ΔT direction in order to enhance the magneto-Seebeck coefficient. B values of −2.9 T to 2.9 T were induced using a super conductance coil cooled by the GM cooler, with a sweep rate of 0.05 T/min, for each thermoelectric property measurement.

RESULTS AND DISCUSSION

The diameter and length of the sintered Bi-Sb specimens were 10.2 mm and 12.3 mm, respectively. The density d was 9.36 g/cm^3, with a relative

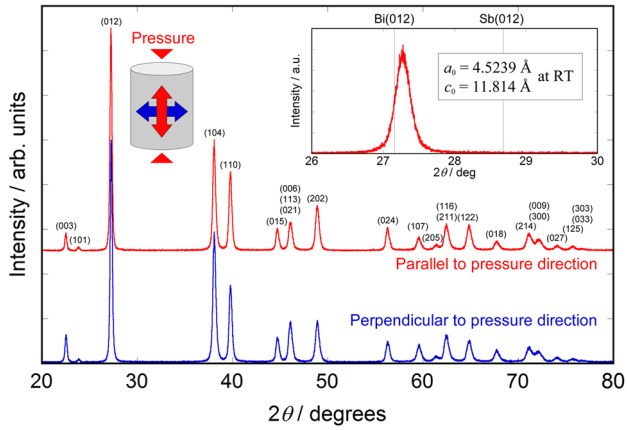

Fig. 2. X-ray diffraction (XRD) patterns of sintered $Bi_{90}Sb_{10}$ alloy measured at two surfaces parallel and perpendicular to pressure direction. Inset: XRD pattern from 26° to 30° around (012) peak.

d of 98% measured using the Archimedean method. The sintered sample was cut using a wire saw, and an XRD measurement was performed on two surfaces parallel and perpendicular to the pressure direction, as shown in Fig. 2. This result shows that the peaks at (003) and (006) for the perpendicular direction measurement were slightly larger than those for the parallel direction, implying that the c-axis was easily oriented perpendicular to the pressure direction. The XRD pattern from 26° to 30° around the (012) peak shown in the inset of Fig. 2 indicates that the peak for the Bi-Sb alloy was shifted in the positive direction by approximately 0.11°, compared to that of pure Bi. Further, there was no peak at the pure Sb position, indicating that the Bi-Sb alloy was successfully synthesized. The lattice constants evaluated from the XRD result were a_0 = 4.524 Å and c_0 = 11.814 Å for a hexagonal crystal system, which are smaller than the pure Bi values of a_0 = 4.546 Å and c_0 = 11.862 Å. These correspond to the reported values for $Bi_{90}Sb_{10}$ of a_0 = 4.522 Å and c_0 = 11.810 Å, which were calculated from data for $a_0 = 4.546–23.84 \times 10^{-4}x$ Å and

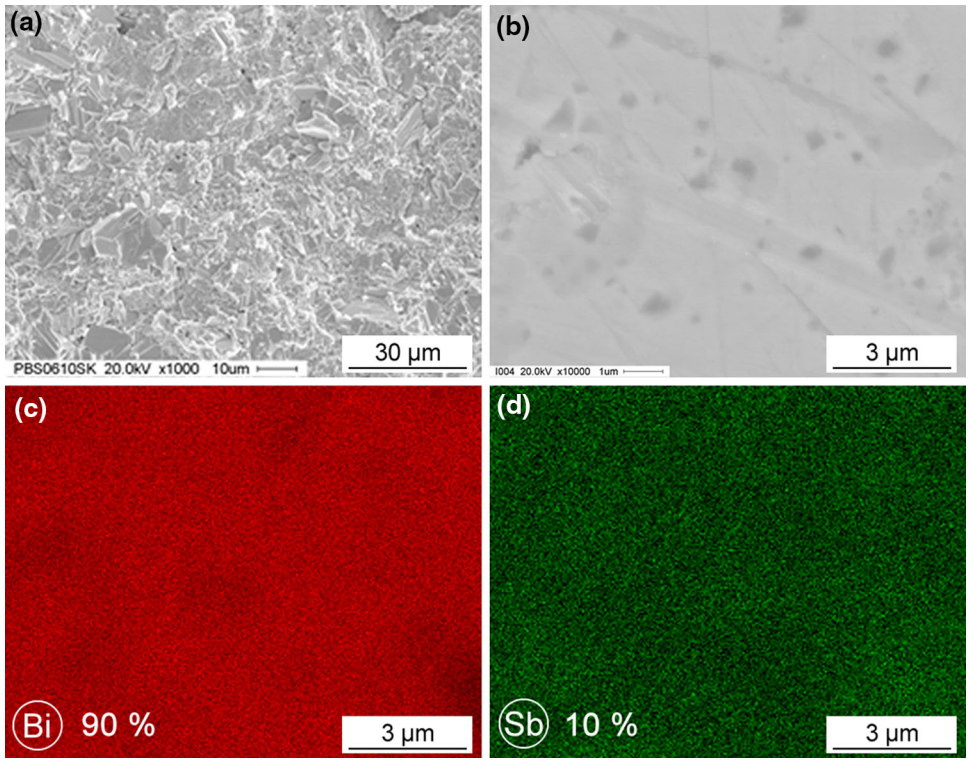

Fig. 3. Scanning electron microscopy (SEM) observation results for sintered $Bi_{90}Sb_{10}$ alloy. SEM micrographs of (a) fracture surface and (b) polished surface. Energy dispersive x-ray spectroscopy mapping analysis results for (c) Bi and (d) Sb observed at area shown in (b).

c_0 = 11.862–51.66 × $10^{-4}x$ Å reported in the literature.[21] Conversely, the Sb concentration was calculated to be 9.2% and 9.3% removed from the measured a_0 and c_0 lattice constants, respectively. These values roughly correspond to 10% of the values obtained from the EDX analysis, meaning that the majority of the Bi and Sb were alloyed.

Figure 3 shows scanning electron microscope (SEM) observation results for the sintered $Bi_{90}Sb_{10}$ alloy. The alloy grain sizes were estimated to be several to several tens of micrometers using the SEM micrograph of the fracture surface shown in Fig. 3a. Very few small vacant spots, supporting the high relative d value of 98%, were observed in the micrograph. Figure 3b–d are, respectively, an SEM micrograph of the polished surface and EDX mapping analyses of Bi and Sb observed at the area shown in (b). Although some spots and scars were observed in the micrograph shown in (c), large segregation was not observed in the EDX mapping results. The Bi and Sb concentrations were analyzed to be 90% and 10%, respectively, using an EDX quantitative analysis, which agrees with the concentrations of the base Bi-Sb alloy.

Figure 4 shows the individual B dependencies of the various thermoelectric properties and ZT from −2.9 to 2.9 T at different T. The ρ values at all T increased symmetrically with the absolute value of B, as shown in Fig. 4a. An increase in electrical resistance through application of an external B is known as magneto-resistance (MR) effect.[22] The ρ at 300 K increased from 2.2 μΩm for the non-B case to 4.0 μΩm under a B of 2.9 T. The 2.9 T to 0 T MR ratio, i.e., $\{\rho(2.9\ \mathrm{T}) - \rho(0\ \mathrm{T})\}/\rho(0\ \mathrm{T})$, was 0.8 at 300 K, and increased with decreasing T to 1.3, 2.3, 4.2, 6.5 and 6.8 for 250 K, 200 K, 150 K, 100 K, and 77 K, respectively. A value of $\{\rho(1.4\ \mathrm{T}) - \rho(0\ \mathrm{T})\}/\rho(0\ \mathrm{T})_{160\mathrm{K}} = 2.9$ has been reported for the $Bi_{88}Sb_{12}$ single crystal, with the conducting direction and B in the trigonal and bisectrix directions, respectively.[4] The $\{\rho(1.4\ \mathrm{T}) - \rho(0\ \mathrm{T})\}/\rho(0)_{150\mathrm{K}} = 1.9$ value obtained in this study for similar conditions to the work cited above was smaller than the reported value for the single crystal. It has been reported that the MR effect on the polycrystal is slightly smaller than that for the single crystal at approximately 150 K.[22] Note that a large difference in the B effect on ρ was not observed for the sintered Bi-Sb alloy and single-crystal cases, because the MR effect does not have strong crystal orientation dependence.[10] The carrier mobility μ of the semi-metal can be evaluated roughly by considering the B dependence of ρ in the low B range. This satisfies the low B approximation.[23]

$$\frac{\rho(B) - \rho(0)}{\rho(B)} = \mu_e \mu_h B^2, \qquad (1)$$

where $\rho(B)$, $\rho(0)$, μ_e, and μ_h are the electrical resistivity under the influence of B and in non-B conditions and the electron and hole carrier mobilities, respectively. This means that the square root of the coefficient of B^2 represents the geometric mean of the electron and hole carrier mobility, i.e., $\mu_m = \sqrt{\mu_e \mu_h}$.

The inset of Fig. 5 shows the B dependence of the electrical resistivity increment $\{\rho(B) - \rho(0)\}/\rho(B)$ at 300 K and the curve fitting result as a function of B^2 under ca. 0.2 T. The estimated coefficient from the fitting curve was $\mu_e\mu_h = 0.68$, such that $\mu_m = 0.825\ m^2\ V^{-1}\ s^{-1}$ at 300 K. This mobility was in the range of that of bulk single-crystal Bi, which is from 0.4 to 1 $m^2\ V^{-1}\ s^{-1}$ at 300 K. Figure 5 shows the T dependence of μ_m, estimated from the B dependence of ρ. Here, μ_m increased with decreasing temperature in proportion to $T^{-1.60}$, which is characteristic of Bi and Bi-Sb alloys. Although the T multiplier of −1.60 is slightly smaller than the value of approximately −2.3 for bulk single-crystal Bi,[24] it is reasonable for the μ_m to decrease at low T, because sintered Bi-Sb was used in this study. Furthermore, it has been reported that the multiplier of T ranges from −1.27 to −1.54 for a Bi single crystal with a small impurity content.[25]

The lattice κ can be expressed as the product of α, d, and the heat capacity C. Here, the measured result of $d = 9.36\ g/cm^3$ is used and C is estimated from the Debye model as[23]

$$C = 9Nk_B\left(\frac{T}{\theta}\right)^3 \int_0^{\theta/T} \frac{\xi^4 e^\xi}{(e^\xi - 1)^2} d\xi, \quad (2)$$

where N, k_B, θ, and ξ are the number of atoms per unit mass, the Boltzmann constant, the Debye temperature, and the integration variable, respectively. The N and θ of the Bi-Sb alloy can be calculated using the Kopp–Neumann law,[26] with

$$N = (1 - z)N_{Bi} + xN_{Sb}, \quad (3)$$

and

$$\theta^{-3} = (1 - z)\theta_{Bi}^{-3} + x\theta_{Sb}^{-3}, \quad (4)$$

where z, N_{Bi}, N_{Sb}, θ_{Bi}, and θ_{Sb} are the Sb concentrations expressed in at.%, the number of atoms per unit mass of Bi and Sb, and the Debye temperatures of Bi and Sb, respectively. The electron contribution to C can be ignored, because it is sufficiently small at the high T range of 77 K to 300 K considered in this study.[23] It was found that the κ values at all T decreased with the absolute value of B, as shown in Fig. 4b. This reduction was caused by decreases in σ, because the phonon conduction is not affected strongly by the external B.[27] When the carrier thermal conductivity was calculated from the measured ρ with a pseudo-Lorentz number of $L = 1.4 \times 10^8\ W\ \Omega/K^2$, the phonon thermal conductivity had no B dependence at any T. Here, L included contributions from not only the electrons and holes, but also the bipolar diffusion.[28] The phonon thermal conductivity at 300 K was estimated to be 2.2 W/mK, as shown in the inset of Fig. 4b, which is comparable with the reported value of ca. 2.0 W/mK for the Bi single crystal.[27] The thermal conductivity ratios $\{\kappa(2.9\ T) - \kappa(0\ T)\}/\kappa(0\ T)$ were −0.19, −0.24, −0.25, −0.27, −0.18 and −0.03 at 300 K, 250 K, 200 K, 150 K, 100 K, and 77 K, respectively.

Figure 4c shows the B dependence of S, i.e., the magneto-Seebeck coefficient. The absolute value of the magneto-Seebeck coefficient at 300 K increased by 38%, from −96.1 μV/K in the non-B case to −133 μV/K under a B of 2.9 T. Although the magneto-Seebeck coefficient at 250 K and 300 K monotonously and symmetrically increased with the absolute value of B up to 2.9 T, an asymmetry dependence known as the Umkehr effect[29] was observed at 77 K, 100 K, and 150 K. The magneto-Seebeck coefficient at 150 K increased monotonously under negative B and began to decrease at approximately 1 T under positive B. Further, the magneto-Seebeck coefficient at 77 K and 100 K increased under a low B, but began to decrease when B was increased. The maximum ratios of the magneto-Seebeck coefficient increase $\{S(B_{opt}) - S(0\ T)\}/S(0\ T)$ were 0.46, 0.46, 0.41, 0.24 and 0.09 at 250 K, 200 K, 150 K, 100 K, and 77 K, respectively; these values are smaller than those of the single crystal. For example, $\{S(1.2\ T) - S(0\ T)\}/S(0\ T)_{300K} = 0.38$ has been reported for the $Bi_{88}Sb_{12}$ single crystal for ΔT and B in the trigonal and binary directions,[10] respectively. This enhancement of the magneto-Seebeck coefficient is larger than our result of $\{S(1.2\ T) - S(0\ T)\}/S(0\ T)_{300K} = 0.24$ for similar conditions. However, $\{S(1.2\ T) - S(0\ T)\}/S(0\ T)_{300K} = 0.20$ has also been reported for the $Bi_{88}Sb_{12}$ single crystal for ΔT and B in the binary and trigonal directions, respectively.[10] The magneto-Seebeck coefficient is strongly dependent on the crystal orientation relative to the ΔT and B. Therefore, there is a possibility that the magneto-Seebeck coefficient differs from that of the single crystal because the grain crystal orientations are random in the sintered Bi-Sb alloy.

Figure 4d shows the B dependence of ZT calculated from the measured thermoelectric properties. At 300 K, ZT increased with the absolute value of B and saturated at approximately 2 T. Further, from 100 K to 250 K, ZT increased at low B but began to decrease as B was increased. At 77 K, ZT monotonously decreased with the absolute value of B. The enhancement of ZT is determined by a balance between the increases in the magneto-Seebeck coefficient and MR. The ZT at high T was well enhanced because the increases in MR and in the magneto-Seebeck coefficient were smaller and larger than those at low T, respectively.

Figure 6a shows the T dependence of the maximum ZT for the applied external B, ZT_{max}, and the ZT in the non-B case, $ZT(0\ T)$. At 77 K, ZT_{max} and $ZT(0\ T)$ were almost identical, because ZT monotonously decreased with the absolute value of B. The

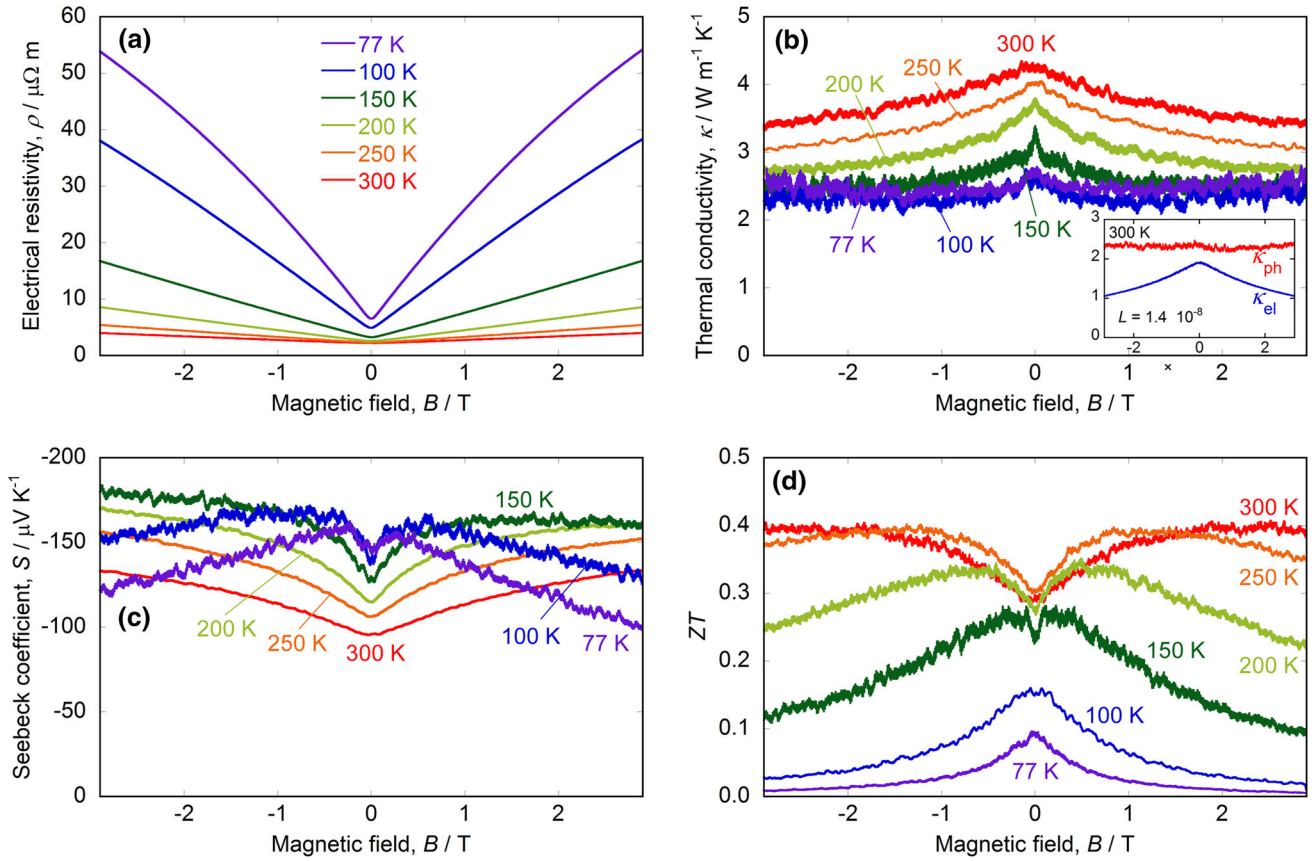

Fig. 4. Magnetic field B dependencies of (a) electrical resistivity ρ, (b) thermal conductivity κ, (c) Seebeck coefficient S, and (d) dimensionless figure of merit ZT, from −2.9 T to 2.9 T at different temperatures. The inset of (b) shows the B dependencies of the electron and phonon thermal conductivities, κ_{el} and κ_{ph}, respectively, at 300 K (Color figure online).

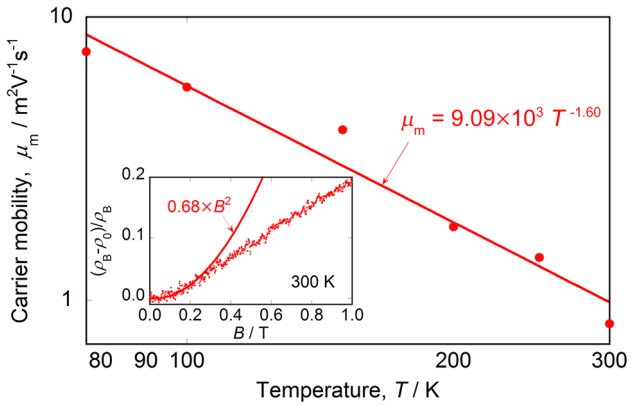

Fig. 5. Temperature dependence of electron and hole mobility geometric mean μ_m. Inset: Electrical resistivity increment under magnetic field $(\rho_B - \rho_0)/\rho_B$ at 300 K and fitting curve.

difference between these ZT increased with T, and the ZT values in the non-B case and for an applied B of 2.5 T at 300 K were 0.30 and 0.41, respectively. Figure 6b shows the $\{ZT_{max} - ZT(0\ T)\}/ZT(0\ T)$ ratio and the optimum magnetic field B_{opt} necessary to obtain ZT_{max}. As shown in the graph, $\{ZT_{max} - ZT(0\ T)\}/ZT(0\ T)$ and B_{opt} increased with T from 1.01 T to 0.1 T at 77 K to 1.37 T and 2.5 T at 300 K, respectively. However, the ZT ratio was ca. 40% less than that of the single crystal at 294 K (2.44),[4] because the magneto-Seebeck coefficient was significantly smaller than that of the single crystal. Thus, the difference between the magneto-Seebeck coefficients of the single crystal and sintered alloy is discussed below, using a calculation model.

The Seebeck coefficient tensor obtained from the Boltzmann equation is expressed as[15]

$$\underline{S_i} = \frac{1}{q}\frac{\int \underline{F_i(\mathbf{k})}\left[-\left(\varepsilon_i(\mathbf{k}) - \varepsilon_{i,F}\right)/T\right]\mathrm{d}\mathbf{k}_i}{\int \underline{F_i(\mathbf{k})}\mathrm{d}\mathbf{k}_i}, \qquad (5)$$

where q, ε_i, $\varepsilon_{i,F}$ and $\mathbf{k}$ are the electric charge, carrier energy, Fermi level, and wave number vector, respectively, and i indicates L or T. The integration variable can be changed from $\mathbf{k}$ to ε_i according to

$$\mathrm{d}\mathbf{k}_T = \left(m_{T,x}m_{T,y}m_{T,z}\right)^{1/2}\frac{4\sqrt{2}\pi}{\hbar^3}\sqrt{\varepsilon_T}\mathrm{d}\varepsilon_T, \qquad (6a)$$

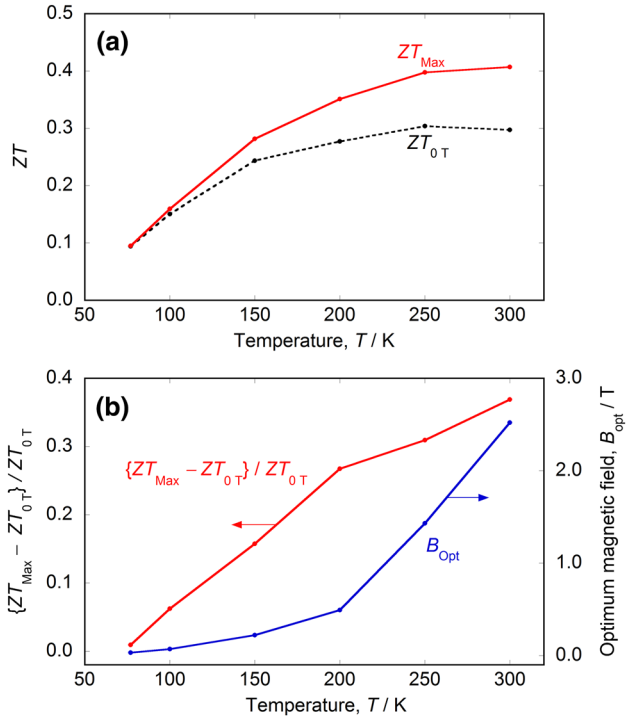

Fig. 6. Temperature dependencies of (a) maximum dimensionless figure of merit ZT under the magnetic field, ZT_{max}, and ZT in the non-magnetic field case, ZT_{0T}. (b) ZT_{max} to ZT_{0T} ratios and optimum magnetic field B_{opt} necessary to obtain ZT_{max}.

$$\mathrm{d}\mathbf{k}_L = \left(\tilde{m}_{L,x}\tilde{m}_{L,y}\tilde{m}_{L,z}\right)^{1/2}\frac{4\sqrt{2}\pi}{\hbar^3}\sqrt{\varepsilon_L\left(1+\frac{\varepsilon_L}{\varepsilon_{gL}}\right)}\left(1+\frac{2\varepsilon_L}{\varepsilon_{gL}}\right)\mathrm{d}\varepsilon_L, \tag{6b}$$

where a tilde on the effective mass indicates that it is an on-diagonal element of the diagonalized effective mass tensor. Non-parabolicity was considered in the calculation at the L-point band using the Lax model.[30,31] Here, the $\underline{F_i(\mathbf{k})}$ at the T and L points are expressed as

$$F_\mathrm{T}(\mathbf{k}) = \frac{\partial f_0}{\partial \varepsilon_\mathrm{T}}\mathbf{v}_\mathrm{T}^t\mathbf{v}_\mathrm{T}\cdot\left(q\underline{B}\underline{\mathrm{m}}_\mathrm{T}^{-1}+\underline{\tau}_\mathrm{T}^{-1}\right)^{-1}, \tag{7a}$$

$$F_\mathrm{L}(\mathbf{k}) = \frac{\partial f_0}{\partial \varepsilon_\mathrm{L}}\mathbf{v}_\mathrm{L}^t\mathbf{v}_\mathrm{L}\cdot\left[q\underline{B}\underline{\mathrm{m}}_\mathrm{L}^{-1}\left(1+\frac{2\varepsilon_\mathrm{L}}{\varepsilon_\mathrm{gL}}\right)^{-1}\left\{1-\frac{4\varepsilon_\mathrm{L}}{3\varepsilon_\mathrm{gL}}\left(1+\frac{\varepsilon_\mathrm{L}}{\varepsilon_\mathrm{gL}}\right)\left(1+\frac{2\varepsilon_\mathrm{L}}{\varepsilon_\mathrm{gL}}\right)^{-2}\right\}+\underline{\tau}_\mathrm{L}^{-1}\right]^{-1}, \tag{7b}$$

respectively, where f_0 is the Fermi–Dirac distribution function, $\mathbf{v}_\mathrm{T}$, $\mathbf{v}_\mathrm{L}$, $\underline{\mathrm{m}_\mathrm{T}}$, $\underline{\mathrm{m}_\mathrm{L}}$, τ_T and τ_L are velocity vectors, effective mass tensors, and relaxation times at the T and L points, respectively, and ε_gL is the direct band gap at the L point. The $\underline{\mathrm{m}_\mathrm{T}}$ and $\underline{\mathrm{m}_\mathrm{L}}$ terms are removed by substituting the following values from the literature on the pure Bi single crystal[32]:

$$\underline{m_\mathrm{T}^*} = \begin{pmatrix}0.064 & 0 & 0\\ 0 & 0.064 & 0\\ 0 & 0 & 0.69\end{pmatrix}m_0, \tag{8a}$$

$$\underline{m_{\mathrm{L,Bi}}^*} = \begin{pmatrix}0.00119 & 0 & 0\\ 0 & 0.263 & 0.0274\\ 0 & 0.274 & 0.00516\end{pmatrix}m_0, \tag{8b}$$

where m_0 is the free electron mass. In addition, the effective mass at the L point is assumed to vary with the energy gap proportionality such that[33]

$$m_\mathrm{L}^* = m_{\mathrm{L,Bi}}^*\frac{\varepsilon_\mathrm{gL}}{\varepsilon_{\mathrm{gL,Bi}}}, \tag{9}$$

where $\varepsilon_{\mathrm{gL,Bi}}$ is the energy gap at the L point on pure Bi. The magnetic field tensor B is related to the external magnetic field $\mathbf{B} = (B_x, B_y, B_z)$ and is defined as

$$\underline{B} = \begin{pmatrix}0 & -B_z & B_y\\ B_z & 0 & -B_x\\ -B_y & B_x & 0\end{pmatrix}. \tag{10}$$

The $\mathbf{v}_\mathrm{T}$ and $\mathbf{v}_\mathrm{L}$ expressions are obtained by multiplying the column vector by the row vector such that

$$\mathbf{v}_\mathrm{T}^t\mathbf{v}_\mathrm{T} = \frac{2\varepsilon_\mathrm{T}}{3}\underline{\alpha_\mathrm{T}'}, \tag{11a}$$

$$\mathbf{v}_\mathrm{L}^t\mathbf{v}_\mathrm{L} = \frac{2\varepsilon_\mathrm{L}}{3}\left(1+\frac{\varepsilon_\mathrm{L}}{\varepsilon_\mathrm{gL}}\right)\left(1+\frac{2\varepsilon_\mathrm{L}}{\varepsilon_\mathrm{gL}}\right)^{-2}\underline{\alpha_\mathrm{L}'}, \tag{11b}$$

where α_i' is expressed as

$$\underline{\alpha_i'} = \begin{pmatrix}\frac{1}{\tilde{m}_{i,x}} & \frac{1}{\sqrt{\tilde{m}_{i,x}\tilde{m}_{i,y}}} & \frac{1}{\sqrt{\tilde{m}_{i,x}\tilde{m}_{i,z}}}\\ \frac{1}{\sqrt{\tilde{m}_{i,y}\tilde{m}_{i,x}}} & \frac{1}{\tilde{m}_{i,y}} & \frac{1}{\sqrt{\tilde{m}_{i,y}\tilde{m}_{i,z}}}\\ \frac{1}{\sqrt{\tilde{m}_{i,z}\tilde{m}_{i,x}}} & \frac{1}{\sqrt{\tilde{m}_{i,z}\tilde{m}_{i,y}}} & \frac{1}{\tilde{m}_{i,z}}\end{pmatrix}. \tag{12}$$

The energy dependencies of τ_T and τ_L are given by

$$\underline{\tau_\mathrm{T}} = \underline{\tau_{\mathrm{T},0}}\left(\frac{\varepsilon_\mathrm{T}(\mathbf{k})}{k_\mathrm{B}T}\right)^r, \tag{13a}$$

$$\underline{\tau_\mathrm{L}} = \underline{\tau_{\mathrm{L},0}}\left(1+\frac{2\varepsilon_\mathrm{L}}{\varepsilon_\mathrm{gL}}\right)\left(\frac{\varepsilon_\mathrm{L}(\mathbf{k})}{k_\mathrm{B}T}\left(1+\frac{\varepsilon_\mathrm{L}(\mathbf{k})}{\varepsilon_\mathrm{gL}}\right)\right)^r, \tag{13b}$$

where $\underline{\tau_{\mathrm{i},0}}$ is a constant tensor with on-diagonal elements only calculated from

$$\underline{\tau_{i,0}} = n|q|\underline{\mu_i}\left(\underline{\sigma_i'}\right)^{-1}, \tag{14}$$

where n, μ_i and σ_i' are the carrier density, carrier mobility tensor, and electronic conductivity tensor, respectively.

The evaluation of n via the Hall effect is complicated, because Bi-Sb has two electron and hole carriers and strong anisotropy in μ_0.[2] In order to evaluate the carrier density and mobility, 12

coefficients should be measured using the single crystal. Therefore, in this study, n was calculated from the band structure with the carrier neutral condition. The T dependence values of the μ_i, which were calculated from values reported in the literature on the Bi single crystal at 77 K and 293 K,[24] were applied to the $Bi_{90}Sb_{10}$ alloy mobility tensor at 300 K. (These values were used because the μ of a Bi-rich Bi-Sb alloy is roughly identical to that of pure Bi.)[34]

$$\underline{\mu_T} = \begin{pmatrix} 22.7\times10^4\ T^{-2.27} & 0 & 0 \\ 0 & 22.7\times10^4\ T^{-2.27} & 0 \\ 0 & 0 & 4.17\times10^4\ T^{-2.28} \end{pmatrix}, \tag{15a}$$

$$\underline{\mu_L} = \begin{pmatrix} 104\times10^4\ T^{-2.22} & 0 & 0 \\ 0 & 6.91\times10^4\ T^{-2.46} & -10.9\times10^4\ T^{-2.33} \\ 0 & -10.9\times10^4\ T^{-2.33} & 76.7\times10^4\ T^{-2.28} \end{pmatrix}. \tag{15b}$$

Here, σ_i' are defined as

$$\underline{\sigma_T'} = \frac{2\sqrt{2}q^2}{3\hbar^3\pi^2}\left(m_{T,x}m_{T,y}m_{T,z}\right)^{1/2}(k_BT)^{3/2} \times \int \frac{\exp(x_T-\zeta_T)}{\{1+\exp(x_T-\zeta_T)\}^2}\underline{\alpha_T'}x_T^{r+3/2}dx_T, \tag{16a}$$

$$\underline{\sigma_L'} = \frac{2\sqrt{2}q^2}{3\hbar^3\pi^2}\left(\tilde{m}_{L,x}\tilde{m}_{L,y}\tilde{m}_{L,z}\right)^{1/2}(k_BT)^{3/2} \times \int \frac{\exp(x_L-\zeta_L)}{\{1+\exp(x_L-\zeta_L)\}^2}\underline{\alpha_L'}\left(x_L\left(1+\frac{k_BTx_L}{\varepsilon_{gL}}\right)\right)^{r+3/2}dx_L. \tag{16b}$$

In addition, the following dimensionless carrier energy and Fermi level were applied in the calculation:

$$x_i = \frac{\varepsilon_i}{k_BT}, \tag{17}$$

$$\zeta_i = \frac{\varepsilon_{i,F}}{k_BT}. \tag{18}$$

The magneto-Seebeck coefficients of the holes at the T point and of the electrons and holes at the L point were calculated using Eqs. 4–17 and the band structure. Here, the effective mass and mobility tensors were diagonalized during the calculation using a proper rotating operation. The Sb-concentration dependencies of the overlap energy Δ_O and the energy gap ε_{gL} in the Bi-Sb alloy at 4.2 K have been reported as[35]

$$\Delta_O = (38 - 5.6z)\ \text{meV}, \tag{19}$$

$$\varepsilon_{gL} = |13.6 - 2.44z|\ \text{meV}. \tag{20}$$

This change in the band structure is caused by alteration of the lattice constant due to the presence of Sb. The Sb concentration dependence of c_0 at 4.2 K has been reported as[21]

$$c_0 = 11.803 - 40.75\times10^{-4}z\ \text{Å}. \tag{21}$$

Thus, the relationship between the band parameters and c_0 can be obtained from Eqs. 18–20 such that

$$\Delta_O = (-1.618\times10^4 - 1.374\times10^3c_0)\ \text{meV}, \tag{22}$$

$$\varepsilon_{gL} = |-7.054\times10^3 + 5.988\times10^2c_0|\ \text{meV}. \tag{23}$$

On the other hand, T also strongly affects the band structure due to the alteration of c_0.[16] However, the relationship between the band structure and T in Bi-Sb alloys has not been reported. Therefore, we estimated the band structure at room temperature from the measured c_0 = 11.814 Å of the sintered $Bi_{90}Sb_{10}$ alloy using Eqs. 21 and 22, where

$$\Delta_O = 52.4\ \text{meV}, \tag{24}$$

$$\varepsilon_{gL} = 20.2\ \text{meV}. \tag{25}$$

The magneto-Seebeck coefficient calculation was performed for six ΔT and **B** conditions. Three main binary, bisectrix, and trigonal axes in the [100], [010], and [001] directions in the Brillouin zone [k_x k_y k_z] were considered in the calculation, as follows:
ΔT//[100], with **B**//[010] or **B**//[001],
ΔT//[010], with **B**//[100] or **B**//[001],
ΔT//[001], with **B**//[100] or **B**//[010].
Furthermore, five scattering factors, r = −0.5, 0.0, 0.5, 1.0 and 1.5, were applied. Figure 7 shows the calculated magneto-Seebeck coefficients for the electron at the L(A)-point Fermi pocket at 300 K. The black solid lines represent the simple average of the six direction conditions, considering that the crystal orientations of the small grains were random in the sintered alloy. Although the simple average is not sufficiently accurate to incorporate all random crystal orientation directions, the error is small because the anisotropy ratio of the maximum to minimum value is ca. 1.5 in this scenario. Therefore, we used a simple average with six degrees of freedom in this study in order to simplify the calculation. The absolute value of the magneto-Seebeck coefficient increased with the absolute value of B at r = −0.5 only, which indicates acoustic phonon potential scattering. The magneto-Seebeck coefficient increased slightly at r = 0.0 and decreased at r = 0.5, 1.0, and 1.5 with the absolute value of B. Thus, the increase in the magneto-Seebeck coefficient could only be explained by acoustic phonon potential scattering. This calculated

result implies that the dominant scattering process in the sintered $Bi_{90}Sb_{10}$ alloy being acoustic phonon potential scattering, is unchanged from that of the single crystal.[31] This result means that the grain size was sufficiently larger than the carrier mean free path by approximately 100 nm at 300 K. The magneto-Seebeck coefficient increased when B was applied along [010], where the cyclotron effective mass was small.

The same calculations were performed on the holes at the L(A) point, the electrons and holes at the L(B) and L(C) points, and the holes at the T-point Fermi pockets. Figure 8a shows the B dependencies of the averaged magneto-Seebeck coefficients at all Fermi pockets. The results show that the magneto-Seebeck coefficients at the L(A), L(B), and L(C) points were almost identical. The absolute value of all the magneto-Seebeck coefficients increased with the absolute value of B, and the increase at the L point was larger than that at the T point. The S value for the contribution from all the Fermi pockets is given by

$$S = \frac{b\{(S_{\mathrm{LA,e}} + S_{\mathrm{LB,e}} + S_{\mathrm{LC,e}})n_{\mathrm{L}} + (S_{\mathrm{LA,h}} + S_{\mathrm{LB,h}} + S_{\mathrm{LC,h}})p_{\mathrm{L}}\} + S_{\mathrm{T,h}}p_{\mathrm{T}}}{b(3n_{\mathrm{L}} + 3p_{\mathrm{L}}) + p_{\mathrm{T}}}, \tag{26}$$

where n_{L}, p_{L}, and p_{T} are the carrier densities of the partial electrons and holes at the L point and of the holes at the T point, respectively, and b corresponds to $\mu_{\mathrm{L}}/\mu_{\mathrm{T}}$. The B dependence of b was ignored, because the change in σ under B was small at 300 K. Figure 8b shows the calculated magneto-Seebeck coefficients for different b and the experimental result. The experimental result quantitatively corresponds to the calculated result of b = 3.3, which is in the range of that of the Bi single crystal (from b = 3.10 for the binary-bisectrix plane to b = 18.4 for the trigonal direction) at 300 K. The average of b in the single-crystal case, considering spheroidal anisotropy, is estimated to be

$$\begin{aligned}\langle b\rangle &= \frac{\int_0^{2\pi}\int_0^{\pi} b\sin\theta \mathrm{d}\theta\mathrm{d}\Phi}{\int_0^{2\pi}\int_0^{\pi}\sin\theta\mathrm{d}\theta\mathrm{d}\Phi},\\ &= \frac{1}{2}\int\left\{\left(\frac{\sin\theta}{3.10}\right)^2 + \left(\frac{\cos\theta}{18.4}\right)^2\right\}^{-\frac{1}{2}}\sin\theta\mathrm{d}\theta,\\ &= 4.41.\end{aligned} \tag{27}$$

Although this b value is larger than our result, this discrepancy is acceptable because the measured σ of the sintered $Bi_{90}Sb_{10}$ alloy differs from that of the single crystal. This means that the measured magneto-Seebeck coefficient of the Bi-Sb alloy was successfully explained by the theoretical calculation, both qualitatively and quantitatively.

The S value at 300 K was explained without considering the B dependence of b. However, the B dependence of σ should be considered at lower T, because ρ has a strong magnetic field dependence. Therefore, it is concluded that the magneto-Seebeck coefficient enhancement in the sintered Bi-Sb alloy is smaller than that of the single crystal because the crystal orientations of the grains were random. Grabov et al. have reported that the magneto-Seebeck coefficient in the single crystal is strongly dependent on the directions of ΔT and B, because the Bi-Sb alloy has strong anisotropy.[9] Experimental results for the magneto-Seebeck coefficient with various Sb concentrations from 2.2% to 40% and T values from 80 K to 200 K have been reported in that paper. However, these results cannot be compared with our calculation, because the band

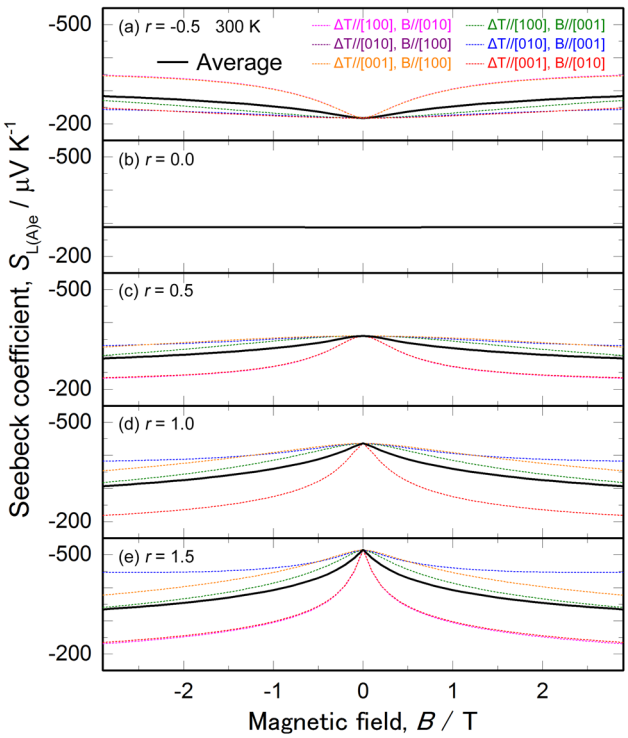

Fig. 7. Calculated temperature dependencies of magneto-Seebeck coefficient of L(A)-point electrons at 300 K with different carrier scattering factors of: (a) −0.5, (b) 0.0, (c) 0.5, (d) 1.0, and (e) 1.5 (Color figure online).

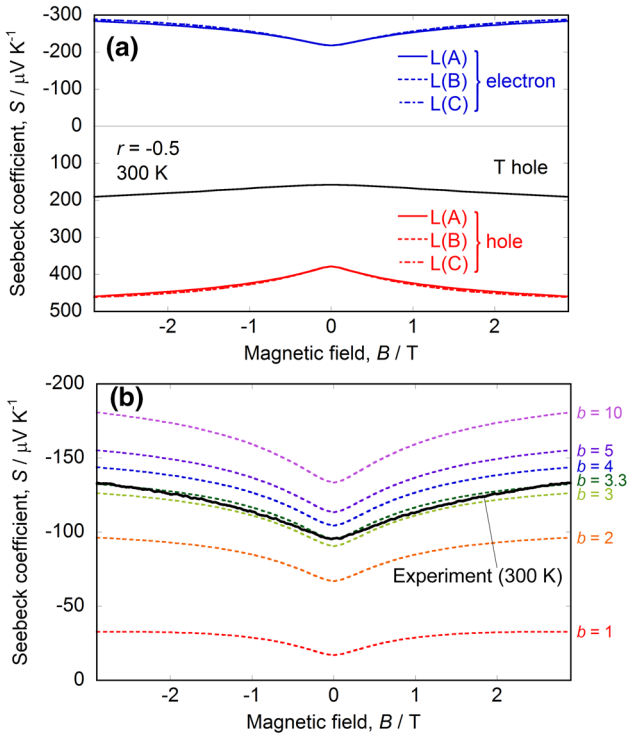

Fig. 8. (a) Magnetic-field dependencies of calculated partial magneto-Seebeck coefficients at all Fermi pockets. (b) Calculated magneto-Seebeck coefficients for different mobility ratios b and experimental result (Color figure online).

structure is unclear in that temperature range. In this study, the band structure at 300 K could be estimated from the lattice constants evaluated from the XRD measurement at room temperature.

Our previous calculation of the magneto-Seebeck coefficient was conducted at 100 K, at which temperature the band structure does not change significantly, and the experimental result could not be explained quantitatively using the carrier neutral condition.[15] On the other hand, this study was successful in providing a quantitative explanation of the experimental result obtained for the carrier neutral condition, by carefully considering the change in the band structure and using the Lax model. It is predicted that the effect of B on the thermoelectric properties is enhanced with decreased effective mass.[15] The effective mass of the Bi-Sb alloy depends on the Sb concentration, and a very small effective mass appears when the Sb concentration is 5%.[34] Therefore, we are planning to study the effective-mass dependence of the magneto-Seebeck coefficient using the established theoretical calculation for a low-temperature range of less than 77 K. Although the B dependence of ρ and κ could not be examined theoretically in this study, ZT will also be estimated in future work, using an improved calculation model. The potential exploitation of the B effect as a means of dramatically enhancing thermoelectric performance will be examined.

Furthermore, the sample size also affects the influence of B on σ and S. It has been reported that the MR does not increase significantly in a small-width sample, and that the magneto-Seebeck coefficient increases to a greater extent in a sample with a high length-to-width ratio.[36] This means that the B effect on the thermoelectric performance will be enhanced for samples with very thin wire shapes, such as nanowires. Our group has successfully developed Bi nanowires of several hundred nanometers in diameter and more than 1 mm in length, which have very high length-to-width ratios.[37] Therefore, a theoretical calculation of the B effect considering the influence of size will be performed, along with an experimental verification using Bi-Sb-based nanowires.

CONCLUSION

The individual B dependencies of the thermoelectric properties of a sintered $Bi_{90}Sb_{10}$ alloy were studied. The examined Bi-Sb alloy was synthesized using the melting method, and the resultant ingot was ground using ball milling. The prepared powder was sintered via the SPS method in order to fabricate a bulk sample, which was then used in the measurement of the B dependence of the thermoelectric properties. The sintered $Bi_{90}Sb_{10}$ alloy grains were several to several tens of micrometers in size; this is sufficiently larger than the carrier mean free path at temperatures of more than 77 K. The electrical resistivity, Seebeck coefficient, and thermal conductivity were evaluated at temperatures from 77 K to 300 K under an external B of up to 2.9 T. The electrical resistivity and Seebeck coefficient increased and the thermal conductivity decreased with the absolute value of B. The results showed that the dimensionless figure of merit at 300 K increased by 37%, from 0.30 in the non-B case to 0.41 under B = 2.5 T. A model calculation of the magneto-Seebeck coefficient based on the Boltzmann equation was also conducted in order to explain the measurement result from a theoretical perspective. Hence, the experimental result for the magneto-Seebeck coefficient was successfully explained both qualitatively and quantitatively by the theoretical calculation. The scattering mechanism was shown to be acoustic phonon potential scattering, and the carrier mobility ratio between the L and T points was found to be 3.3; these results correspond to the single-crystal characteristics. In future, using the established calculation model, high-performance thermoelectric materials will be developed that will be calibrated using adjustments to the effective mass and size based on the B effect.

ACKNOWLEDGEMENTS

The author would like to thank Mr. Ryoei Homma of Saitama University and Mr. Masaru Kunii and Mr. Hirotaka Nishiate of AIST for their assistance with this research. This research was supported in

part by JSPS KAKENHI (Grant numbers: 26886016 and 15H04142) and the Inamori Foundation, Izumi Science and Technology Foundation.

REFERENCES

1. G.E. Smith and R. Wolfe, *J. Appl. Phys.* 33, 841 (1962).
2. B. Lenoir, H. Scherrer, and T. Caillat, *Semicond. Semimet.* 69, 101 (2001).
3. S. Tang and M.S. Dresselhaus, *J. Mater. Chem. C* 2, 4710 (2014).
4. R. Wolfe and G.E. Smith, *Appl. Phys. Lett.* 1, 5 (1962).
5. H. Scherrer and S. Scherrer, *Thermoelectrics Handbook: Macro to Nano*, ed. D.M. Rowe (Boca Raton, FL: CRC, 2006), p. 27.
6. M.V. Vedernikov and V.L. Kuznetsov, *CRC Handbook of Thermoelectrics*, ed. D.M. Rowe (Boca Raton, FL: CRC, 1995), p. 609.
7. W.M. Yim and A. Amith, *Solid-State Electrons* 15, 1141 (1972).
8. P. Jandl and U. Birkholz, *J. Appl. Phys.* 76, 7351 (1994).
9. V.M. Grabov and O.N. Uryupin, *Thermoelectrics Handbook: Macro to Nano*, ed. D.M. Rowe (Boca Raton, FL: CRC, 2006), p. 28.
10. S. Tanuma and M. Sakurai, *J. Adv. Sci.* 7, 163 (1995).
11. M.E. Ertl, G.R. Pfister, and H.J. Goldsmid, *Brit. J. Appl. Phys.* 14, 161 (1963).
12. C.B. Thomas and H.J. Goldsmid, *Phys. Lett.* 27A, 369 (1968).
13. T. Komine, Y. Ishikawa, A. Suzuki, H. Shirai, and Y. Hasegawa, *Proceedings of 22nd International Conference on Thermoelectrics*, p. 500 (2003).
14. Y. Hasegawa, T. Komine, Y. Ishikawa, A. Suzuki, and H. Shirai, *Jpn. J. Appl. Phys.* 43, 35 (2004).
15. T. Teramoto, T. Komine, S. Yamamoto, M. Kuraishi, R. Sugita, Y. Hasegawa, and H. Nakamura, *J. Appl. Phys.* 104, 053714 (2008).
16. E.E. Mendez, Ph.D. thesis, Massachusetts Institute of Technology (1979).
17. B. Leinoir, A. Demouge, D. Perrin, H. Sherrer, S. Scherrer, M. Cassart, and J.P. Michenaud, *J. Phys. Chem. Solids* 56, 99 (1995).
18. W.P. Lin, D.E. Wesolowski, and C.C. Lee, *J. Mater. Sci.* 22, 1313 (2011).
19. Y. Hasegawa, D. Nakamura, M. Murata, H. Yamamoto, and T. Komine, *Rev. Sci. Ins.* 81, 094901 (2010).
20. R. Homma, Y. Hasegawa, H. Terakado, H. Morita, and T. Komine, *Jpn. J. Appl. Phys.* 54, 026602 (2015).
21. P. Cucka and C.S. Barrett, *Acta Cryst.* 15, 865 (1962).
22. C.L. Chien, F.Y. Yang, K. Liu, D.H. Reich, and P.C. Searson, *Phys. Rev. Lett.* 82, 3328 (1999).
23. C. Kittel, *Introduction to Solid State Physics* (New York: Wiley, 1966).
24. G.A. Saunders and Z. Sumengen, *Proc. R. Soc. Lond. A* 329, 453 (1972).
25. Y. Hasegawa, I. Ishikawa, T. Saso, H. Shirai, H. Morita, T. Komine, and H. Nakamura, *Phys. B* 382, 140 (2006).
26. M.S. Narayana and N.G. Krishna, *Phys. Stat. Sol. (a)* 202, 2731 (2005).
27. B.S. Farag and S. Tanuma, *ISSP Technical Report,* Ser. B No. 18 (1976).
28. C.F. Gallo, B.S. Chandrasekhar, and P.H. Sutter, *J. Appl. Phys.* 34, 144 (1963).
29. R. Wolfe and G.E. Smith, *Phys. Rev.* 129, 1086 (1963).
30. B. Lax, *Rev. Mod. Phys.* 30, 122 (1958).
31. J.P. Heremans and O.P. Hansen, *J. Phys. C: Solid State Phys.* 12, 3483 (1979).
32. Y.M. Lin, Master's thesis, Massachusetts Institute of Technology (2000).
33. N.B. Brandt and S.M. Chudinov, *Sov. Phys. JETP* 32, 815 (1971).
34. B. Lenoir, M. Cassart, J.-P. Michenaud, H. Scherrer, and S. Scherrer, *J. Phys. Chem. Solids* 57, 89 (1996).
35. J. Heremans, D.L. Partin, C.M. Thruch, G. Karczewski, M.S. Richardson, and J.K. Furdyna, *Phys. Rev. B* 48, 11329 (1993).
36. Y. Hasegawa, H. Nakano, H. Morita, A. Kurokouchi, K. Wada, T. Komine, and H. Nakamura, *J. Appl. Phys.* 101, 033704 (2007).
37. M. Murata, D. Nakamura, Y. Hasegawa, T. Komine, T. Taguchi, S. Nakamura, V. Jovovic, and J.P. Heremans, *Appl. Phys. Lett.* 94, 192104 (2009).